# Noninvasive Evaluation of Retinal Leakage Using OCT

Rui Bernardes[1,2], Torcato Santos[1], Pedro Serranho[2], Conceição Lobo[1,2,3] and José Cunha-Vaz[1,2]

1. Center of New Technologies for Medicine, Association for Innovation and Biomedical Research on Light and Image (AIBILI), Coimbra, Portugal.
2. Institute of Biomedical Research on Light and Image, Faculty of Medicine, University of Coimbra, Coimbra, Portugal.
3. Coimbra University Hospital, Coimbra, Portugal.

*R. Bernardes – Association for Innovation and Biomedical Research on Light and Image, Azinhaga Sta. Comba, Celas, 3000-548 Coimbra, Portugal (e-mail: rcb@aibili.pt / rmbernardes@fmed.uc.pt)

*Index Terms* – optical coherence tomography, retinal leakage analyzer, fluorescein angiography, blood-retinal barrier.

**Grant**: This study is supported in part by the *Fundação para a Ciência e a Tecnologia* (FCT) under the research project PTDC/SAU-BEB/103151/2008 and program COMPETE (FCOMP-01-0124-FEDER-010930).

**Clinical Trials Registration**: This study is registered at ClinicalTrials.gov (ID: NCT00797524).

ABSTRACT

**Purpose:** To demonstrate the association between changes in the blood-retinal barrier identified by fluorescein leakage and those in the optical properties of the human retina determined by optical coherence tomography and show how these changes can be quantified and their location identified within the retina.

**Methods:** Two imaging techniques were applied: the retinal leakage analyzer, to map blood-retinal barrier function into intact or disrupted regions, and optical coherence tomography, to measure refractive index changes along the light path within the human ocular fundus.

**Results:** A total of 140 comparisons were made, 77 between areas from regions receiving the same classification (intact or disrupted blood-retinal barrier) and 63 between areas of regions receiving distinct classifications, from 4 pathological cases: two eyes with nonproliferative diabetic retinopathy and two eyes with wet age-related macular degeneration. In all cases, the distribution of optical coherence tomography data between regions of intact and regions of disrupted blood-retinal barrier, identified by the retinal leakage analyzer, were statistically significant different ($p < 0.001$). In addition, it was found that not all retinal layers contributed equally to those differences.

**Conclusions:** Using a novel method to analyze optical coherence tomography data, we showed that it may be possible to quantify differences in the extracellular compartment in eyes with retinal disease and alterations of the blood-retinal barrier. Based on quantitative techniques, our findings demonstrated the presence of indirect information on the blood-retinal barrier status whithin noninvasive optical coherence tomography data.

## I. Introduction

Diabetes mellitus (DM) is a multifactorial disease that has a large social and economic impact in the active working population in western countries. In addition, the prevalence of those with diabetes are increasing worldwide; current estimates project more than 438 million people will have diabetes by 2030, representing a global prevalence of 7.8%. [1] Among the complications of diabetes, diabetic retinopathy (DR) remains the leading cause of vision loss. [1]

Age-related macular degeneration (AMD) is another highly prevalent retinal disorder that is associated with vision loss. AMD is characterized by aging changes in the photoreceptors, retinal pigment epithelium (RPE), Bruch's membrane and choroid. [2]

Both diabetic retinopathy and AMD are associated with increased permeability of the blood-retinal barrier (BRB) and retinal edema.

The human BRB exists at two distinct levels. The inner BRB consists of the tight junctions of the endothelial cells of the vascular network, and the outer BRB consists of the tight junctions of the RPE. The BRB function is to block the penetration of substances from the bloodstream into the extracellular space of the retina, therefore preventing access to the retinal neurons of substances that may put vision at risk.

The status of the BRB function, either intact or disrupted, is traditionally assessed qualitatively by fluorescein angiography (FA) and quantitatively by vitreous fluorophotometry.

Vitreous fluorophotometry was introduced in 1975 to measure fluorescein leakage from the bloodstream into the human vitreous by Cunha-Vaz et al. [3] and recently developed further by Lobo et al. [4] and Bernardes et al. [5] using confocal microscopy and named retinal leakage analyzer (RLA). However, technical difficulties and the need for dedicated instrumentation and technically skilled personnel has limited the use of these instruments as imaging modalities to research centers. Subsequently, conventional fluorescein angiography is still the technique of choice for the qualitative assessment of fluorescein leakage in the human ocular fundus, only surpassed in number by color fundus photography.

The major drawback of the available methods to evaluate BRB function is the fact that they are invasive. An exogenous dye (sodium fluorescein) is intravenously administered to patients, and minimal adverse reactions occur in 5% of the cases. Death too may occur in the first 24 to 48 hours in 1 of 220,000 cases. [6] As a result, fluorescein angiograms and vitreous fluorophotometry can be performed only in the presence of a physician at sites with life support equipment.

In this way, the objective of the present study was to evaluate the feasibility of the non-invasive assessment of the BRB function status through changes in the optical properties of the retina associated to BRB disruption. Moreover, we intended to demonstrate that these changes can be quantified and identified by its location within the retina.

## II. Material and methods

To demonstrate the existence of BRB function status information within OCT data, two imaging techniques were applied. One, an invasive technique (the retinal leakage analyzer), uses intravenous fluorescein administration to map BRB function into intact or disrupted regions. The second, a non-invasive technique, uses OCT, an imaging modality that visualizes the retinal structure in 3D by measuring refractive index changes along the light path within the human ocular fundus.

Four eyes of four patients (representative of well defined clinical cases) were examined by RLA to compute maps of BRB function and by OCT to demonstrate local changes in the optical properties of the retinal tissue in relation to BRB functional status. Two patients were diagnosed with nonproliferative diabetic retinopathy (the right eye of a 64-year-old man [DR 1] and the left eye of a 53-year-old man [DR 2]), and two patients were diagnosed with wet AMD (the left eye of a 70-year-old woman [AMD 1] and the right eye of a 68-year-old woman [AMD 2]).

It was thought that retinal regions with disrupted BRB will result, as compared to retinal regions with intact BRB, in an increased extracellular space resulting from the loss of barrier properties of either the endothelial or pigment epithelial layers, or both.

The tenets of the Declaration of Helsinki were followed, and approval from the institutional ethics and review board was obtained. Informed consent was obtained from all the patients (clinical trial identifier at http://www.clinicaltrials.gov/: NCT00797524).

### A. Retinal Leakage Analyzer (RLA)

The RLA was proposed by Lobo et al. [4] based on a modified prototype confocal scanning laser ophthalmoscope. An update to this process was proposed by the same group [5], which now uses a commercially available instrument, the Heidelberg Retina Angiograph (HRA, Heidelberg Engineering, Heidelberg, Germany), that has been modified for this purpose.

In brief, the HRA I (classic version) allows the acquisition of 32 confocal planes along 7 mm, from the vitreous to the choroid. Each fluorescein angiogram is 225.8 μm apart from the next, and each one is composed of 256x256 or 512x512 pixels.

After correcting for saccades it is possible to compute a fluorescence intensity profile from the vitreous to the choroid. By analyzing this profile, the amount of fluorescein present in the vitreous and the amount of fluorescein leakage from the bloodstream into the human vitreous, can be determined. [5]

A map can thus be built that indicates the amount of leakage and consequently the status of the BRB, either intact or disrupted, respectively for the normal or increased amount of fluorescein leakage, in relation to the amount of fluorescein leakage computed from a healthy reference population.

Moreover, this system (RLA) allows a fundus reference to be computed, which enables information from the BRB function to be correlated with any imaging modality for which a fundus reference image can be computed (e.g., the OCT and color fundus photography). This correlation can be achieved by co-registering both fundus images through common intrinsic fiducial markers as vessels bifurcations and/or crossovers (Fig. 1).

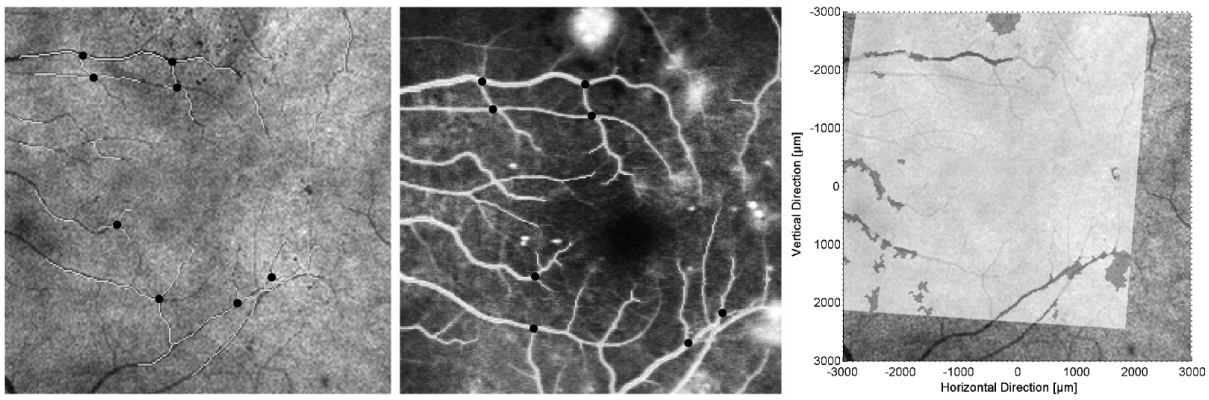


*Figure 1: Image co-registration. Fundus references from OCT (left) and RLA (center). Dots show the location of characteristics common to both images. Right: Map of blood-retinal barrier (BRB) status (grayed regions indicates disrupted BRB) projected over the OCT fundus reference.*

B. Optical Coherence Tomography (OCT)

A non-invasive diagnostic imaging technology, OCT, provides cross-sectional images of the retinal tissue. Its working principle is analogous to that of ultrasonography except that OCT uses light rather than sound. [7-11]

The high-definition spectral domain Cirrus OCT (Carl Zeiss Meditec, Dublin, CA, USA) was used in this work. The system has 5-µm depth resolution, 20-µm transverse resolution and a scanning speed of 27000 A-scans per second, allowing for a volumetric ocular fundus scan of either 512x128x1024 or 200x200x1024 voxels from a 6000x6000x2000 $\mu m^3$ volume, the lateral, azimuthal and axial directions, respectively (Fig 2). It allows users access to an unprecedented detail of the retinal structures from subjects *in vivo*.

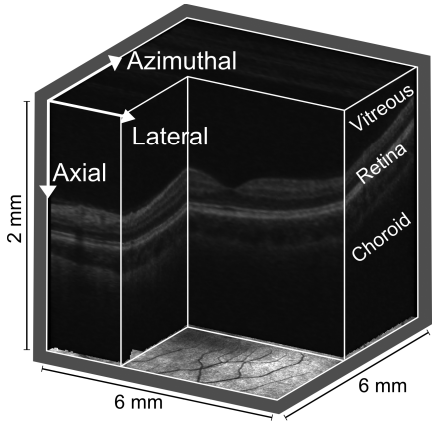


*Figure 2: Optical coherence tomography volumetric data display. The fundus image reference underneath the volume is automatically computed from the volume and corresponds to the integral (sum) along the axial direction.*

The OCT uses some terminology from ultrasonography; therefore, an A-scan is a set of depth-wise readings for a particular location in the ocular fundus, and a B-scan is an image assembled from a set of side-by-side A-scans along a line (Fig. 3).

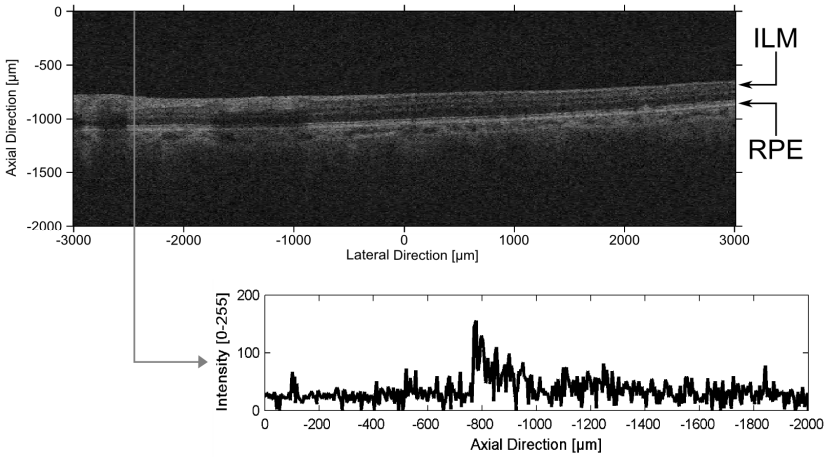


*Figure 3: Optical coherence tomogram (B-scan image - top) and the intensity plot of an A-scan (bottom). Top: the dark upper area region of the image represents the vitreous, immediately followed by the retina (delimited by the inner limiting membrane [ILM] and by the retinal pigment epithelium [RPE]), the RPE and choroid.*

Traditionally, OCT has been used to assess structural information from the ocular fundus, allowing the identification of cyst-like structures, retinal detachments, changes in the RPE and macular holes, among other changes. Also, OCT has been used to measure retinal thickness, either total thickness from the inner limiting membrane (ILM) to the RPE, or the thickness of specific retinal layers using advanced image-processing techniques (e.g., the retinal fiber layer or the photoreceptor layer).

OCT readings result from reflections and/or light scattering due to refractive index changes along the light path and are therefore dependent on the content and structural organization of the eye. Any change in those elements will result in a change in OCT readings.

C. Histograms

To demonstrate OCT differences between two regions within the same eye/scan, associated with changes in BRB function, we computed the statistical changes in OCT data using a well-known technique to characterize data distributions. This technique, the histogram, is the plot of the number of times a particular value is found in a distribution. Since each OCT datum is coded in a byte, the allowed range for the data is from zero to 255.

To capture the changes within the retina, the histograms were built from ocular fundus data in a volume delimited between the ILM and the RPE for a region within the fundus reference.
Histograms are sensitive to changes in data, as it implies a change in the shape of the histogram, and were therefore a natural choice for the current purpose.

D. Histogram/Probability Density Function Differences

We checked for OCT differences in the OCT findings within the same eye (with changes from the healthy reference condition based on the RLA) and scan.
The two eyes with diabetic retinopathy and the two eyes with AMD were examined through the RLA to compute maps of BRB function and OCT.
Based on the co-registration of the respective fundus images (from the OCT and from the RLA) it was possible to compute OCT data histograms from regions of intact or disrupted BRB (according to the classification received from the RLA) in volumes delimited by the ILM (top) and the RPE (bottom). Regions of the same size were chosen to include the same number of A-scans to not bias the results.
Histograms were thereafter normalized (divided) by the total number of OCT data readings to become probability density functions (PDF).
Probability density functions of two distinct areas to be compared were brought into alignment by the respective maximum value. A difference-profile was then built between probability density functions of two distinct areas to be compared and the sum of the squared differences (SSD) was computed. Consequently, we compared PDFs of OCT data from areas: a) of the same region type (intact or disrupted BRB), and; b) of different region types (intact to disrupted BRB).

E. Differences by Layer

Additionally, to detect if any retinal layer(s) contributed more to any differences, we split the retina into seven equally spaced layers between the ILM and the RPE, and numbered them from top to

bottom (the number 1 starts at the ILM and the number 7 ends at the RPE; Fig. 4). In general, this approach placed retinal vascular network within layers 1 to 3.

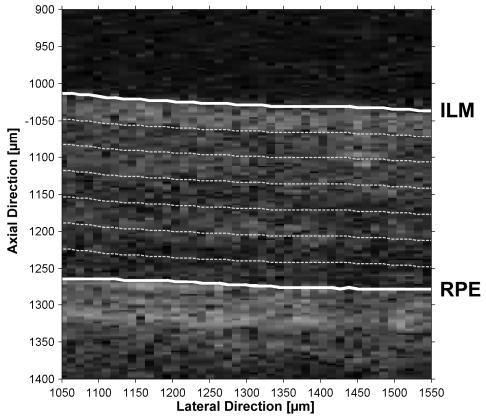


*Figure4: The retina is split into seven equally spaced layers between the inner limiting membrane (ILM, layer 1) and the retinal pigment epithelium (RPE, layer 7), from top to bottom.*

F. Data Analysis

Data analysis was performed through the SPSS Inc. (version 16.0, Chicago, IL, USA) to determine data normality (Shapiro-Wilk and Kolmogoroff-Smirnoff tests) and differences between groups (Kruskal-Wallis, Tukey Post-Hoc and Mann-Whitney tests). For all tests we considered a significance of 5%.

III. Results

Four pathological cases were used to demonstrate local changes in the optical properties of the retinal tissue in relation to BRB functional status. Patients were examined by RLA to compute maps of BRB function (intact vs. disrupted BRB), as shown in figure 5, overlaid to the respective OCT fundus references.

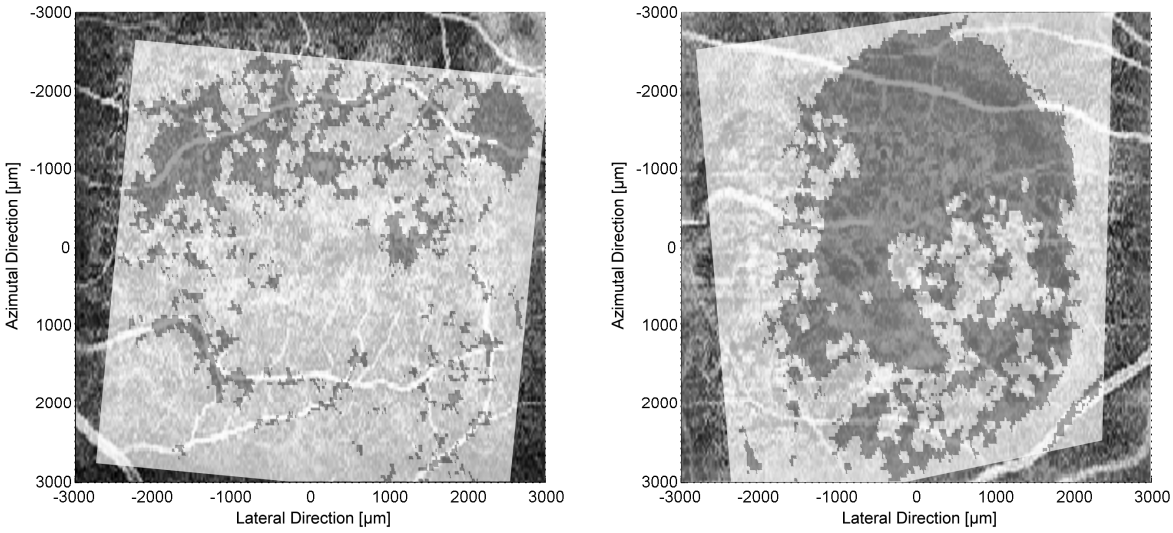


*Figure 5: Maps of retinal leakage analyzer indicating blood-retinal barrier disruption (grayed regions) overlaid to OCT fundus reference images after image co-registration based on intrinsic fiducial markers. DR 2 is the left eye of a man age 53 years, and AMD 2 is the right eye of a woman age 68 years, left and right, respectively.*

From each eye, areas from intact BRB and areas from localized disrupted BRB regions were identified (Fig. 6).

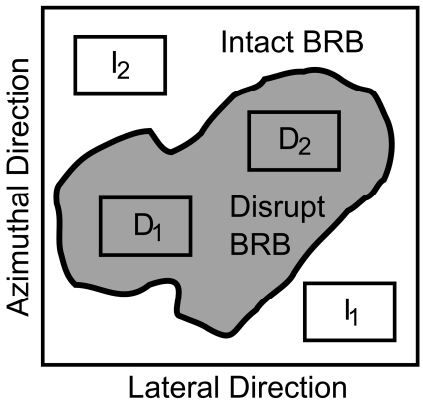


*Figure 6: Illustration of the areas considered for each analysis, areas within the blood-retinal barrier (BRB) intact (I) region and areas within the disrupted (D) region.*

A. Probability Density Function Differences

Two possibilities emerged from the classification of the BRB functional status, a comparison of OCT PDF from two areas from the same region, receiving the classification of intact or disrupted BRB, and a comparison of OCT PDF from one area from a region of intact BRB and one area from a region of disrupted BRB. Each area was defined to include 5000 A-scans, the number found to be enough to represent the local statistical properties of the OCT data.

In this way, OCT PDF differences and the respective sum of squared differences were computed between similar regions ($Diff_{similar}$) and between distinct regions ($Diff_{distinct}$).

Plots in figure 7 demonstrate the differences found. These are summarized in Table 1 through the SSD.

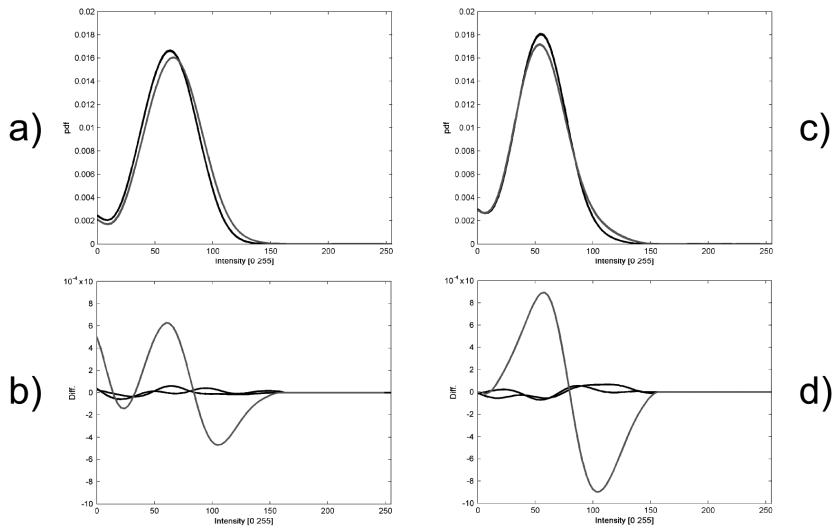


*Figure 7: Eye with diabetic retinopathy (DR 2; a & b) and eye with age-related macular degeneration (AMD 2; c & d). Probability density function (PDF) plots (a & c) for four areas, two from intact and two from disrupted BRB regions, respectively dark and gray lines (plots of similar regions overlap, hence only two lines are noticeable). PDF differences are shown in plots b & d, with dark lines representing differences between similar BRB regions (either intact or disrupted BRB) and the gray line represents the differences between dissimilar BRB regions (intact/disrupted BRB regions).*

Table 1: Summary of differences by type ($Diff_{similar}$ – between two areas of the same region type, $Diff_{distinct}$ – between two areas of distinct region types). The lower the sum of squared differences (SSD) the higher the similarity between PDF profiles (mean±SD (number of comparisons)).

| Patient ID | Sum of squared differences (SSD) ($x10^{-9}$) | |
|---|---|---|
| | $Diff_{similar}$ m±SD (N) | $Diff_{distinct}$ m±SD (N) |
| DR #1 | 25.06 ± 21.17 (21) | 609.22 ± 35.90 (7) |
| DR #2 | 8.95 ± 12.38 (22) | 61.80 ± 14.54 (14) |
| AMD #1 | 7.72 ± 9.42 (25) | 201.87 ± 35.62 (30) |
| AMD #2 | 1.78 ± 1.30 (9) | 81.38 ± 13.14 (12) |

Data from Table 1 were tested to check for the respective normality through both the Shapiro-Wilk and Kolmogoroff-Smirnoff normality tests to find $Diff_{similar}$ and $Diff_{distinct}$ to be non-normally distributed ($p < 0.001$) therefore requiring the use of non-parametric tests (Kruskal-Wallis test).

Considering the two difference groups, a $p < 0.001$ (Kruskal-Wallis test) was found thus rejecting the null hypothesis (that the location parameters of the distribution are the same in each group) an the Mann-Whitney test found the difference between was statistically significant ($p < 0.001$).

These findings allowed us to conclude that differences within regions receiving the same classification, either intact or disrupted BRB, differed statistically from the differences between regions receiving classifications of intact or disrupted BRB status, respectively $Diff_{similar}$ and $Diff_{distinct}$. Thus, different optical properties of the human retina were found in relation to changes in BRB function.

B. Differences by Layer

After splitting the retina into seven equally spaced layers between the ILM and the RPE, a similar analysis to that cited was performed for each layer to identify which presented the most significant differences. Table 2 presents the SSD by layer.

Table 2: Summary of differences by layer (1 to 7) and difference type. The lower the sum of squared differences (SSD) the higher the similarity between probability density function profiles (mean±SD (number of comparisons)).

| Patient ID | Sum of squared differences (SSD) ($x10^{-9}$) | | |
|---|---|---|---|
| | Layer | $Diff_{similar}$ m±SD (N) | $Diff_{distinct}$ m±SD (N) |
| DR #1 | 1 | 10.64 ± 9.85 (21) | 1705.77 ± 116.09 (7) |
| | 2 | 25.37 ± 21.21 (21) | 1962.24 ± 123.93 (7) |
| | 3 | 16.41 ± 12.05 (21) | 218.60 ± 42.19 (7) |
| | 4 | 21.45 ± 20.61 (21) | 876.56 ± 50.67 (7) |
| | 5 | 25.43 ± 22.07 (21) | 234.09 ± 58.07 (7) |
| | 6 | 38.55 ± 38.96 (21) | 348.40 ± 59.00 (7) |
| | 7 | 34.34 ± 32.83 (21) | 131.20 ± 25.66 (7) |
| DR #2 | 1 | 16.90 ± 14.70 (22) | 471.38 ± 101.18 (14) |
| | 2 | 13.33 ± 10.70 (22) | 802.78 ± 84.34 (14) |
| | 3 | 6.86 ± 4.37 (22) | 157.52 ± 32.26 (14) |
| | 4 | 14.06 ± 13.37 (22) | 106.19 ± 28.13 (14) |
| | 5 | 16.18 ± 13.39 (22) | 56.55 ± 17.37 (14) |
| | 6 | 17.92 ± 14.44 (22) | 190.42 ± 27.20 (14) |
| | 7 | 3.65 ± 2.26 (22) | 64.18 ± 11.53 (14) |
| AMD #1 | 1 | 10.23 ± 8.16 (25) | 291.24 ± 83.38 (30) |
| | 2 | 11.45 ± 8.40 (25) | 833.59 ± 107.55 (30) |
| | 3 | 8.27 ± 9.33 (25) | 9.68 ± 7.82 (30) |
| | 4 | 17.31 ± 15.09 (25) | 60.16 ± 29.92 (30) |
| | 5 | 10.18 ± 10.06 (25) | 32.74 ± 11.75 (30) |
| | 6 | 13.33 ± 15.56 (25) | 48.28 ± 18.97 (30) |
| | 7 | 6.45 ± 4.02 (25) | 13.56 ± 6.79 (30) |
| AMD #2 | 1 | 15.01 ± 14.88 (9) | 190.60 ± 66.62 (12) |
| | 2 | 12.99 ± 13.41 (9) | 182.62 ± 40.94 (12) |
| | 3 | 3.14 ± 2.32 (9) | 333.84 ± 23.94 (12) |
| | 4 | 5.39 ± 2.89 (9) | 60.70 ± 14.57 (12) |
| | 5 | 26.03 ± 24.32 (9) | 23.41 ± 14.93 (12) |
| | 6 | 15.13 ± 18.52 (9) | 31.47 ± 24.17 (12) |
| | 7 | 7.00 ± 3.65 (9) | 65.13 ± 15.70 (12) |

Data were found to have a non-normal distribution by the Shapiro-Wilk and Kolmogoroff-Smirnoff normality tests.

Considering the two difference groups, a Kruskal-Wallis test was made within each layer to again reject ($p < 0.001$ in all layers) the null-hypothesis that the distributions behave the same.

A $p < 0.001$ (Kruskal-Wallis test) was found, thus rejecting the null hypothesis (that the location parameters of the distribution are the same in each group), and the Tukey Post-Hoc test proposed the existence of three subsets, one composed of layers 3 to 7 (pairwise $p > 0.256$), one composed of layers 1 ($p < 0.001$) and one composed of layers 2 ($p < 0.001$), being the differences more significant in layer 2, then in layers 1, and then in the remaining group of layers.

## IV. Discussion and Conclusions

Our findings showed that using this method to analyze OCT data it is possible to quantify differences in the extracellular compartment in eyes with retinal disease and alterations of the BRB.

Reliable detection of localized changes in the extracellular space offer a non-invasive method that may replace available methods that identify breakdown of the BRB and need intravenous administration of tracer materials.

As reported by Ouyang et al., the volume of the extracellular compartment of the neurosensory retina in the normal eye is regulated by the retinal capillary endothelial cell tight junctions and RPE cell tight junctions (i.e., the inner and outer BRB), as well as by the pumping function of both the endothelial and RPE cells. [12] This intraretinal fluid can accumulate in the extracellular space of the retina where there is loss of functional integrity of the BRB. This accumulation of intracellular fluid is ubiquitous in most retinal diseases, such as diabetic retinopathy and advanced AMD, and the degree of retinal edema is used to monitor disease progression and to make clinical management decisions.

Recently, while referring to the treatment of neovascular AMD, Chakravarthy et al. [13] noted that in some clinical practices the availability of innovative noninvasive imaging tools led to the adoption of algorithms not requiring angiographies and that clinicians are now willing to base their diagnoses on noninvasive techniques, namely on the "…tomographic evidence of fluid in the macular tissues."

The quest for an *in vivo* assessment of BRB function has been a major objective of our research group and many others since the initial identification of the BRB in 1966. [4, 5, 14]

In this study, we have demonstrated the presence of indirect information on BRB status using non-invasive OCT data based on quantitative techniques. We also used the RLA to identify regions of intact and disrupted BRB and analyzed the tissue reflectance/scattering distribution between these regions to find a clear dissimilarity. These differences may offer a way to quantify localized areas of retinal edema.

The use of OCT imaging is gaining acceptance in clinical practice because it is non-invasive and it provides detailed information on the structure of the human ocular fundus. It has also been used by

Wehbe and co-workers [15] to assess blood flow measurement, and by Bizheva and co-workers [16] to evaluate changes in optical properties of the retina due to light stimuli.

Additional research may reveal a new functionality for the OCT that may have an impact on the way patients, especially diabetic patients, are followed up by their ophthalmologist.

## V. ACKNOWLEDGMENT

The authors would like to thanks Dr. Melissa Horne and Carl Zeiss Meditec (Dublin, CA, USA) for their support on getting access to OCT data, and AIBILI Clinical Trial Center technicians for their support in managing data, working with patients and performing scans.

VI. References


1. International Diabetes Federation. Diabetes and impaired glucose tolerance. Global burden. http://www.diabetesatlas.org/content/diabetes-and-impaired-glucose-tolerance (accessed August 26, 2010)]
2. Retina Study Group. *AMD – Age-related macular degeneration*.. 1st ed. Loures, Portugal: Théa Portugal SA, 2010.
3. Cunha-Vaz J, Goldberg M, Vigantas C, Noth J. Early detection of retinal involvement in diabetes by vitreous fluorophotometry. Ophthalmology. 1979;86:264-75.
4. Lobo C, Bernardes R, Santos F, Cunha-Vaz J. Mapping retinal fluorescein leakage with confocal scanning laser fluorometry of the human vitreous. Arch Ophthalmol. 1999;117:631-7.
5. Bernardes R, Dias J, Cunha-Vaz J. Mapping the human blood-retinal barrier function. IEEE Trans Biomed Eng. 2005;52:106-16.
6. Alfaro V, Gómez-Ulla F, Quiroz-Mercado H, Figueroa M, Villalba S (eds). *Retinopatía diabética - Tratado médico quirúrgico*. 1st ed. MAC LINE, S.L., 2006.
7. Drexler W, Morgner U, Kärtner F, Pitris C, Boppart S, Li X, Ippen E, Fujimoto J. In vivo ultrahigh-resolution optical coherence tomography. Optics Lett. 1999; 24:1221-3.
8. Drexler W, Morgner U, Ghanta R, Kärtner F, Schuman J, Fujimoto J. Ultrahigh-resolution ophthalmic optical coherence tomography. Nat Med. 2001;7:502-7.
9. Bouma B, Tearney G. Handbook of Optical Coherence Tomography, New York: Marcel Dekker, Inc., 2002.
10. Fujimoto J. Optical coherence tomography: Principles and applications. Rev Laser Eng. 2003;31:635-42.
11. Schuman J. Spectral domain optical coherence tomography for glaucoma. (an AOS Thesis) Trans Am Ophthalmol Soc. 2008;106:426-58.
12. Ouyang Y, Keane P, Sadda S, Walsh A. Detection of cystoid macular edema with three-dimensional optical coherence tomography versus fluorescein angiography. Invest Ophthalmol Vis Sci. 2010 Mar 31 [Epub ahead of print].

13. Chakravarthy U, McGimpsey S, McAvoy C. How baseline assessment of AMD lesion type influences clinical decisions and outcomes. Retinal Phys. 2010 July: 27-33.

14. Shakib M, Cunha-Vaz J. Studies on the permeability of the blood-retinal barrier. IV. Role of the junctional complexes of the retinal vessels on the permeability of the blood-retinal barrier. Exp Eye Res. 1966;5:229-34.

15. Wehbe H, Ruggeri M, Jiao S, Gregori G, Puliafito C, Zhao W. Automatic retinal blood flow calculation using spectral domain optical coherence tomography. Optics Express. 2007;15:15193-206.

16. Bizheva K, Pflug R, Hermann B, Povazay B, Sattmann H, Qiu P, Anger E, Reitsamer H, PopovS, Taylor J, Unterhuber A, Ahnelt P, Drexler W. Optophysiology: Depth-resolved probing of retinal physiology with functional ultrahigh-resolution optical coherence tomography. Proc Natl Acad Sci USA. 2006;103:5066-71.